Surface crystal field at the Er/Si(111) interface studied by soft-x-ray linear dichroism

P. Castrucci,* F. Yubero, F. C. Vicentin,† J. Vogel, and M. Sacchi
Laboratoire pour L'Utilisation du Rayonnement Electromagnetique, Centre Universitaire Paris-Sud, 91405 Orsay, France
(Received 4 April 1995; revised manuscript received 23 June 1995)

We have measured the $M_{4,5}$ edges of Er in submonolayer coverages of Er on Si(111), using linearly polarized x rays. The observed dichroism has been related to the surface crystal field and interpreted quantitatively in the hypothesis of an axial perturbation. The free ion $^4I_{15/2}$ ground state is split over ≈ 25 meV, the lowest level being of $|\pm\frac{15}{2}\rangle$ symmetry. The results are compared to those of a previous experiment on Dy/Si(111).

I. INTRODUCTION

The theory of polarization-dependent x-ray absorption (dichroism) was initially developed for the study of magnetic effects.[1] More recently, dichroism with linearly polarized light has also been proposed as a probe of crystalline electric field (CEF) effects[2–4] and has been applied to surface layers of Dy deposited on Si(111).[2]

An atom adsorbed on a substrate experiences a strongly asymmetric environment with a finite charge density on one side and vacuum on the other. The corresponding CEF shows a dominant axis of symmetry perpendicular to the surface, which basically determines the splitting of the free atom degenerate levels into a new perturbed scheme. Various techniques can give information about CEF splitting, and notably inelastic neutron scattering (INS), but, when a surface layer is to be studied, most of them fail because of lack of sensitivity. However, thanks to the high cross sections involved, measurements at the $M_{4,5}$ edges of rare earths (RE) can be easily performed on layers with a density of the order of 10^{13} atoms cm^{-2}. The relation between surface crystal fields and x-ray linear dichroism (XLD) has been discussed in previous works[2,5,6] and will be briefly recalled in Sec. II.

We have measured XLD for several submonolayer coverages of Er on Si(111). RE-Si interfaces and alloys have attracted large interest,[7] both fundamental and technological, for their magnetic and electrical properties. Most RE form silicides that grow epitaxially on Si(111) and have very low (≈ 0.35 eV) Schottky barriers[8] on *n*-type Si, with potential applications as infrared detectors and integrated Ohmic contacts. Er, in particular, forms a defective disilicide of approximate stoichiometry $ErSi_{1.7}$, which presents a hexagonal structure[9] formed by alternate stacking of Er and Si planes along the *c* axis. The *ab* plane presents a mismatch of only 1.2% on the Si(111) surface, and the epitaxial growth of $ErSi_{1.7}$ on Si(111) has been extensively investigated.

We have used XLD to investigate the crystal-field-induced splitting of the $^4I_{15/2}$ ground state of Er when the ion is located at the Si(111)7×7 surface. The measurements were performed on as-deposited as well as annealed layers, and the results are compared to those of a previous study on Dy/Si(111). The two sets of data can be coherently explained within a simplified model supposing a CEF of $C_{\infty v}$ symmetry, a result that gives experimental evidence to the relation between crystal fields and linear dichroism.

II. MODEL CALCULATION

The $M_{4,5}$ absorption edges of Er and of all the RE have been calculated in an atomic model several years ago.[10] The atomic model works very well also for the ion in the solid state as long as only the $3d \rightarrow 4f$ transitions are considered, which represent the most intense contribution to the $M_{4,5}$ edges. In this picture, the RE is considered as an ion that has lost its outermost $(5d6s)^m$ electrons (usually $m=3$). Of all the possible transitions between the initial state $3d^{10}4f^n$ and the final state $3d^9 4f^{n+1}$, only those satisfying the dipole selection rules for photon absorption are retained. Indicating with (J,M_J), $(1,q)$, J',M_J') the angular momentum and its projection on the quantization axis for the initial state, the photon, and the final state, respectively, the selection rules are given by $|J-1| \le J' \le J+1$ (or $\Delta J = 0, \pm 1$) and $M_J' - M_J = q$ (or $\Delta M_J = 0, \pm 1$).

For the Er^{3+} free ion, the Hund's rules ground state is $^4I_{15/2}$, hence $2J+1=16$-fold degenerate with M_J values between $-\frac{15}{2}$ and $+\frac{15}{2}$. In Fig. 1, the lines of the bar diagram for Er^{3+}, calculated with Cowan's Hartree-Fock program,[11,12] are reported. In order to fit the experimental unpolarized Er spectrum, different Lorentzian broadenings were used according to the ΔJ value of each line:[13,14] $2\Gamma = 0.50$, 0.35, and 0.30 eV for $\Delta J = -1$, 0, and 1, respectively. An overall Gaussian broadening of $2\sigma = 0.4$ eV was introduced to account for the experimental resolution on the photon energy. The comparison between the calculated and the experimental unpolarized spectra, also given in Fig. 1, shows a general good agreement. The unpolarized spectrum was taken on a polycrystalline Er compound, featuring no dichroism.

The relation between the presence of a perturbing field and the polarization dependence of the absorption can be easily established in the hypothesis of a perturbation weak with respect to the spin-orbit coupling (first-order perturbation theory). In this case, the ground state $|J,M_J^j\rangle$, degenerate for the $2J+1$ values of M_J^j, is split

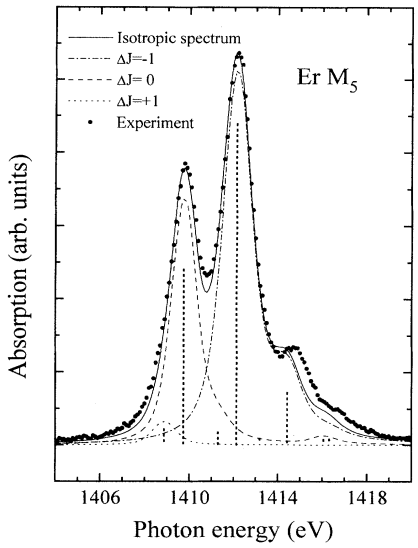

FIG. 1. Comparison between the experimental (dots) and calculated (continuous line) Er M_5 spectrum. The three ΔJ-selected components are also reported.

by the perturbation into the new states $|\Phi_J^i\rangle = \sum_j a_{ij}|M_J^j\rangle$ of energy E_i (J remains a good quantum number). Indicating with $\sigma_J^{q,i}$ the free ion cross section for the transitions from an initial state $|J,M_J^i\rangle$ induced by photons of polarization q, and with $n_i(T)$ the occupation number of the $|\Phi_J^i\rangle$ state at temperature T given by the Boltzmann distribution, one has for the polarization- and T-dependent cross section in the presence of a perturbation

$$s_J^q(T)=\sum_i n_i(T)\sum_j |a_{ij}|^2\sigma_J^{q,j} .$$

To introduce explicitly the polarization dependence, $\sigma_J^{q,j}$ can be written as a function of the ΔJ-selected components $\sigma_{J,K}$ (with $K=J'-J=0,\pm1$) and the $3j$ symbols for the composition of the angular momenta,

$$s_J^q(T)=\sum_K\sum_i\sum_j n_i(T)|a_{ij}|^2 \times \begin{pmatrix} J+K & 1 & J \\ -(M_J^j+q) & q & M_J^j \end{pmatrix}^2 \sigma_{J,K} ,$$

where i and j run over the possible $2J+1$ wave functions $|\Phi_J^i\rangle$ and $|M_J^j\rangle$, respectively, and K over the three possible $J'-J$ values. The three $\sigma_{J,K}$ components for the Er M_5 edge are also reported in Fig. 1.

In the notation of the Stevens's operator equivalents,[15] the CEF Hamiltonian $H_{\rm CEF}$ can be written as

$$H_{\rm CEF}=\sum_{n,m} B_n^m O_n^m=\sum_{n,m}\theta_n A_n^m\langle r^n\rangle O_n^m , \quad (1)$$

where A_n^m are the crystal-field parameters, containing the information about the charge distribution around the ion, $\langle r^n\rangle$ are the integrals of the radial part of the electronic wave functions, and θ_n are the Stevens's factors, also denoted α_J, β_J, and γ_J for $n=2$, 4, and 6, respectively. They are specific to each ion, and depend on the orbital momentum and occupation number of the unfilled shell, as well as on J. O_n^m are the Stevens's operator equivalents acting on the angular part of the wave functions.

The number of nonvanishing terms in Eq. (1) depends on the point symmetry of the ion site. When the symmetry is dominated by the axial term, fourth- and sixth-order components can be neglected, or introduced as second-order perturbations (see, for example, the paper by Peschel and Fulde[16] about the Pr surface).

We have interpreted our data for Er submonolayers on Si(111) assuming a purely axial symmetry ($C_{\infty v}$) for the CEF, with the axis of rotation along the [111] direction of the substrate. In $C_{\infty v}$, we can write[15]

$$H_{\rm CEF}=B_2^0O_2^0=B_2^0[3M_J^2-J(J+1)] . \quad (2)$$

The perturbation splits the $2J+1$ degenerate levels according to the modulus but not the sign of M_J. For half-integer J values, as for Er^{3+}, this leads to $(2J+1)/2$ doublets, separated in energy according to

$$E_i-E_j=3B_2^0\{(M_J^i)^2-(M_J^j)^2\} .$$

Since the $\{a_{ij}\}$ coefficients are fixed by symmetry arguments, B_2^0 is the only free parameter to fit the model calculation to our data: its sign determines the lowest-lying level (either $|\pm\frac{1}{2}\rangle$ or $|\pm\frac{15}{2}\rangle$ for Er^{3+}), hence the angular dependence of the absorption spectra; its absolute value gives the total energy spread of the perturbed levels

$$\Delta E_{\rm total}=3|B_2^0|[(\tfrac{15}{2})^2-(\tfrac{1}{2})^2]=168|B_2^0| ,$$

hence the temperature dependence of the dichroism.

III. EXPERIMENTAL DETAILS

The experiment was carried out at beamline SA-22 of the storage ring Super ACO (LURE, Orsay). A double-crystal monochromator with two beryl ($10\bar{1}0$) crystals allowed us to cover the photon energy range including the $M_{4,5}$ edges of Er with a resolving power of about 3000. To have a degree of linear polarization close to 1, the portion of the beam emitted within ±15 μrad around the ring plane was selected. The presence of two Bragg reflections close to 35° is an additional guarantee for a high rate of linear polarization.

All the measurements were performed in an ultrahigh vacuum chamber (base pressure $<1\times10^{-10}$ mbar) equipped with low-energy electron diffraction (LEED) and Auger analyzers. The Si(111) substrate was cleaned by Ar sputtering and annealed up to 1100 °C till LEED showed a sharp 7×7 pattern and Auger no sign of contaminants.

Er was evaporated by electron bombardment of a high-purity ingot placed in a tungsten basket. Typical evaporation rates, as monitored by a quartz balance, were 0.5 Å/min in a pressure of 1×10^{-9} mbar.

For most of the submonolayer Er/Si interfaces, LEED inspection showed the persistence of the 7×7 reconstruction of the substrate surface in the as-deposited layers.

For annealed layers, superstructures like 2×2 and $\sqrt{3}\times\sqrt{3}$ were sometimes observed, but were not reproducible. The Auger inspections performed immediately after the sample preparation always indicated a very clean surface, while spectra taken about 2 h later showed a relevant amount of oxygen, roughly proportional to the Er deposit.

A thick silicide sample (~ 60 Å) was prepared by reactive deposition, i.e., by evaporating Er on a Si substrate kept at 550 °C. The sample was subsequently annealed for 1 min at 800 °C. Before and after this annealing, the LEED pattern was characterized by the sharp $\sqrt{3}\times\sqrt{3}$ reconstruction typical of the Si-defective ordered phase $ErSi_{1.7}$ (Ref. 17).

The absorption spectra were measured for each sample at different angles between the light polarization vector and the surface normal, ranging between 10° (grazing incidence) and 90° (normal incidence).

As an indirect measure of the absorption process, we collected the total electron yield (TEY) emitted from the sample surface using a channeltron in pulse counting mode. This technique presents a high surface sensitivity and is particularly suited for studying submonolayer coverages. As a drawback, angular-dependent saturation effects in TEY have been observed at the $M_{4,5}$ edges of RE (Refs. 18 and 19), but they do not affect our measurements on submonolayer coverages.

IV. RESULTS AND DISCUSSIONS

A. Submonolayer coverages

XLD measurements have been performed for several submonolayer coverages between 0.1 and 0.3 ML as a function of thermal treatment and sample temperature. All the films prepared and measured in the same conditions gave equivalent results with high reproducibility, regardless of the specific thickness. This lack of thickness dependence indicates that the ion/substrate interaction determines the XLD, with little influence of the Er-Er lateral correlation.

The thermal treatment, on the contrary, has a large influence on the polarization dependence. Figure 2 compares the spectra taken for an as-deposited (0.25 ML) and annealed (0.1 ML, 1 min 550 °C) sample, both measured at room temperature. For each sample we measured at least four different light-to-surface geometries. The fitting procedure, according to the model described in Sec. II, was always applied to the grazing incidence spectrum in order to determine B_2^0. Spectra for other angles were then calculated without introducing further parameters and compared to the experiment in order to check the quality of the fit. The continuous lines in Fig. 2 correspond to $B_2^0=-0.10$ meV and $B_2^0=-0.15$ meV for the as-deposited and annealed layers, respectively. With an error bar of ±0.01 meV, these values are representative of our entire set of submonolayer samples, and within our assumption of a $C_{\infty v}$ symmetry, entirely determine the crystal-field level scheme of the RE ions. The negative sign of B_2^0 indicates that the lowest-lying level is $|\pm\frac{15}{2}\rangle$ and the total energy spread is 25 ± 2 meV

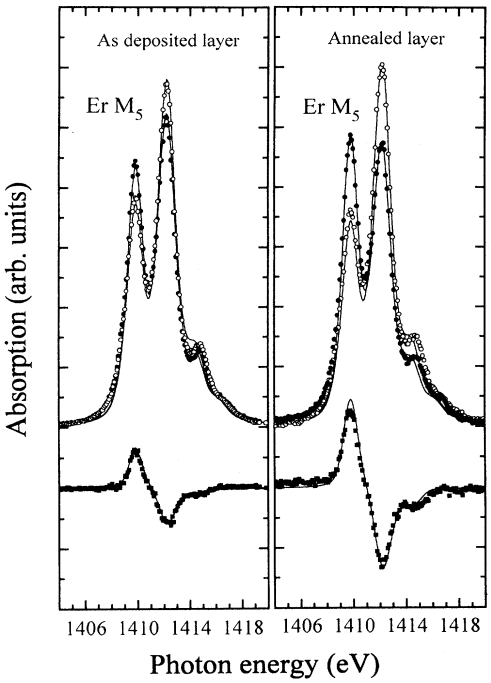

FIG. 2. Polarization-dependent absorption spectra at the Er M_5 edge for a RT-deposited (0.25 ML) and an annealed (0.1 ML, 1 min at 550 °C) layer on Si(111). Open circles: normal incidence spectra ($q=\pm1$). Filled circles: grazing incidence spectra ($q=0$). The curves at the bottom (filled squares) are the differences between grazing and normal incidence. Continuous lines are best fits based on the atomic calculations and crystal-field model discussed in Sec. II. For each sample, the parameter B_2^0 has been optimized on the grazing incidence spectrum.

for the annealed layers. Taking the tabulated values[20] of $\langle r^2\rangle$ and α_J for Er [$0.666a_0^2$ and $2^2/(3^2\times5^2\times7)$, respectively] gives $A_2^0=-88$ meV $a_0^{-2}\simeq10^3$ K a_0^{-2} (a_0 being the Bohr radius).

The lower value of B_2^0 for as-deposited layers should not be taken as indicative of a weaker crystal field, but rather of a distribution of Er sites at the surface. An increased linear dichroism after annealing was already reported for the Dy/Si(111) system. In that case, a combined x-ray absorption (XAS)/photoemission spectroscopy study was also carried out:[21] the increased dichroism was always accompanied by a narrowing of the $4f$ photoemission structures and associated to the evolution towards a single site occupation for the RE ion.

For one sample, we measured, in rapid succession, the normal incidence spectrum at room temperature (RT) and at $T\simeq150\pm10$ K: the two values obtained for B_2^0 agreed within 5%, i.e., within the error bar given above. Contamination of the Er layer prevented a more detailed study versus temperature since we observed that, even for a base pressure of $\sim5\times10^{-11}$ mbar, the lifetime of our samples did not exceed 2 h.

B. Erbium silicide

For the thick $ErSi_{1.7}$ layer only the normal incidence data can be used since, as reported for other RE and

transition metals,[18,19,22] the TEY is affected by a strong angular-dependent saturation. By *thick* layer we mean a layer whose thickness is large with respect to the field of view of XAS in TEY, estimated to be a few tens of Å.

Data collected at $T=150$, 300, and 1000 K are shown in Fig. 3. The $T=1000$ K spectrum is indistinguishable from the unpolarized one, as expected when the temperature is high enough to uniformly populate all the levels of the multiplet. The inset of Fig. 3 shows the spectra, calculated in a $C_{\infty v}$ symmetry, that gave the best fit over the entire T range (experimental data included six temperatures between 150 and 1000 K). The corresponding value of B_2^0 is -0.04 meV, giving a total splitting $\Delta E_{\text{tot}} \simeq 7$ meV and $A_2^0 = -25$ meV a_0^{-2}.

The crystal-field splitting of the Er^{3+} ground state in the silicide has been investigated by other techniques,[23] including INS and magnetization measurements. The results for both bulk and thin (300 Å) film samples could be explained taking a B_2^0 of 13 μeV, a factor 3 smaller than the value we deduced from the linear dichroism measurements. A possible origin for this discrepancy is that our analysis considers only the axial term of second order, while in Ref. 23 also fourth- and sixth-order terms are included. These terms are, however, at least two orders of magnitude smaller than B_2^0. A second possible reason is that XLD measured in TEY is intrinsically surface sensitive. This may enhance the surface contribution to the dichroism, which, as shown before, gives a much larger value for B_2^0. RE silicides, though, are normally Si terminated, which would make even the topmost Er layer equivalent to the others in terms of nearest neighbors.

As a test for internal consistency of linear dichroism applied to crystal-field studies, we compared the results obtained for Er silicide and Dy silicide, which present the same local environments. For Dy (nine $4f$ electrons with a $^6H_{15/2}$ ground-state configuration), we obtain $B_2^0 = -0.11 \pm 0.01$ meV. Considering that for Dy $\langle r^2 \rangle = 0.762 a_0^2$ and $\alpha_J = -2/(3^2 \times 5 \times 7)$, we obtain $A_2^0 = -21 \pm 2$ meV$/a_0^2$, which compares very well to the value for Er ($A_2^0 = -25$ meV$/a_0^2$). We also note that, for the same environment and hence crystal-field parameters, Er^{3+} and Dy^{3+} show opposite ordering of the sublevels, with a $|\pm\frac{15}{2}\rangle$ ground state for the former and $|\pm\frac{1}{2}\rangle$ for the latter. This is related to the opposite sign of the Stevens's factor α_J for the two ions.

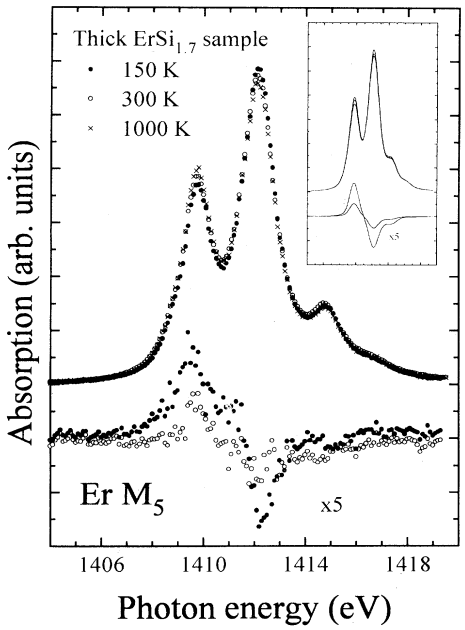

FIG. 3. Temperature dependence of the normal incidence M_5 spectrum of Er in a thick Er silicide layer grown on Si(111). The differences between 1000 and 150 K and 1000 and 300 K are reported at the bottom. The inset shows the corresponding spectra calculated in $C_{\infty v}$ symmetry with $B_2^0 = 40$ μeV.

V. CONCLUDING REMARKS

We have measured the $3d$ absorption spectrum of Er for several Er/Si interfaces, using linearly polarized photons. Large variations occur as a function of the angle between the polarization vector and the surface normal ([111] direction of the Si substrate). No thickness dependence was observed in the submonolayer regime, while thermal treatments have important effects on the dichroism. We have interpreted our experimental results in terms of the splitting of the $^4I_{15/2}$ free ion ground state induced by a crystal field of axial symmetry. Within this framework, we have determined the lowest level to be of $|\pm\frac{15}{2}\rangle$ character, with a total splitting of about 25 meV and B_2^0 parameter of -0.15 meV. Based on these results one expects that ordered submonolayers of Er on Si(111) should present large magnetocrystalline anisotropy, with favored perpendicular magnetization. This follows from the fact that, at $T=0$ K, only the $|\pm\frac{15}{2}\rangle$ state is occupied: it cannot be split by a magnetic field acting in the surface plane, while a field along the surface normal separates it into two states, $|-\frac{15}{2}\rangle$ and $|+\frac{15}{2}\rangle$, giving rise to a magnetic moment of $9\mu_B$. This large anisotropy will be smoothed at finite temperatures, but perpendicular magnetization will remain favored. The same considerations apply to the epitaxial silicide layers, in agreement with the results obtained using other techniques.[23]

We have observed linear dichroism also in a thick $ErSi_{1.7}$ layer epitaxially grown on silicon. Analyzing the results in the same axial CEF hypothesis gives a much smaller splitting ($\Delta E_{\text{total}} \simeq 7$ meV). A comparison has been made with a Dy-silicide layer, where (for the same environment) a reversed level scheme with ground state $|\pm\frac{1}{2}\rangle$ is determined. The different behavior of the two RE ions is related to the opposite signs of their second-order Stevens's factors. The values for the crystal-field parameters A_2^0 obtained with XLD for the two RE silicides agree very well.

The application of soft-x-ray linear dichroism to the study of crystal-field effects presents, in our view, two peculiarities that can turn, for certain systems, into two major advantages: the high sensitivity to little amounts of material and the element selectivity. In addition to the case of submonolayers presented here, also buried layers and multicomponent systems can take advantage of this technique.

ACKNOWLEDGMENTS

This work received financial support from the European Community under Contract No. SC1-CT91-0630. F.C.V. and M.S. acknowledge the financial support from CNPq (Brazil) in the context of a RHAE contract for international exchange.

---

*Permanent address: Dipartimento di Matematica e Fisica, Università di Camerino, Via Madonna delle Carceri, 62032 Camerino (MC), Italy.

†Permanent address: Laboratorio Nacional de Luz Sincrotron (LNLS), Cx. Postal 6192, 13081-970 Campinas SP, Brazil.

[1]B. T. Thole, G. van der Laan, and G. A. Sawatzky, Phys. Rev. Lett. **55**, 2086 (1985); J. B. Goedkoop, B. T. Thole, G. van der Laan, G. A. Sawatzky, F. M. F. deGroot, and J. C. Fuggle, Phys. Rev. B **37**, 2086 (1988).

[2]M. Sacchi, O. Sakho, F. Sirotti, and G. Rossi, Appl. Surf. Sci. **56-58**, 1 (1992); M. Sacchi, O. Sakho, and G. Rossi, Phys. Rev. B **43**, 1276 (1991).

[3]J. B. Goedkoop, Ph.D. thesis, University of Nijmegen, 1989.

[4]P. Carra, H. König, B. T. Thole, and M. Altarelli, Physica B **192**, 182 (1993).

[5]J. Vogel, M. Sacchi, F. Sirotti, and G. Rossi, Appl. Surf. Sci. **65/66**, 170 (1993).

[6]R. J. H. Kappert, J. Vogel, M. Sacchi, and J. C. Fuggle, Phys. Rev. B **48**, 2711 (1993).

[7]F. P. Netzer, J. Phys. Condens. Matter **7**, 991 (1995), and references therein.

[8]K. N. Tu, R. D. Thompson, and B. Y. Tsaur, Appl. Phys. Lett. **38**, 626 (1981).

[9]J. A. Knapp and S. T. Picraux, Appl. Phys. Lett. **48**, 466 (1986).

[10]B. T. Thole, G. van der Laan, J. C. Fuggle, G. A. Sawatzky, R. C. Karnatak, and J.-M. Esteva, Phys. Rev. B **32**, 5107 (1985).

[11]R. D. Cowan, *The Theory of Atomic Structure and Spectra* (University of California Press, Berkeley, 1981).

[12]The line shapes reported in Fig. 1 were calculated starting from the model discussed in Ref. 11, using the computer program developed at the Universities of Groningen and Nijmegen (The Netherlands) (B. T. Thole, B. G. Searle, J. B. Goedkoop, and R. J. H. Kappert).

[13]J. Vogel, Ph.D. thesis, University of Nijmegen 1994.

[14]H. Ogasawara, A. Kotani, and B. T. Thole, Phys. Rev. B **50**, 12 332 (1994).

[15]M. T. Hutchings, in *Solid State Physics: Advances in Research and Applications,* edited by H. Ehrenreich, F. Seitz, and D. Turnbull (Academic, New York, 1964), Vol. 16, p. 227.

[16]I. Peschel and P. Fulde, Z. Phys. **259**, 145 (1973).

[17]F. Arnaud d'Avitaya, A. Perio, J.-C. Oberlin, Y. Campidelli, and J. A. Chroboczek, Appl. Phys. Lett. **54**, 2198 (1989).

[18]O. Sakho, M. Sacchi, F. Sirotti, and G. Rossi, Phys. Rev. B **47**, 3797 (1993).

[19]J. Vogel and M. Sacchi, J. Electron Spectrosc. Relat. Phenom. **67**, 181 (1994).

[20]P. Fulde, in *Handbook on the Physics and Chemistry of Rare Earths,* edited by K. A. Gschneidner and L. Eyring (North-Holland, Amsterdam, 1979), p. 295.

[21]O. Sakho, F. Sirotti, M. de Santis, M. Sacchi, and G. Rossi, Appl. Surf. Sci. **56-58**, 568 (1992).

[22]G. van der Laan and B. T. Thole, J. Electron Spectrosc. Relat. Phenom. **46**, 123 (1988).

[23]J. A. Chroboczek, A. Briggs, W. Joss, S. Auffret, and J. Pierre, Phys. Rev. Lett. **66**, 790 (1991).